The role of grain boundaries and denuded zones for tritium retention in high-dose neutron irradiated beryllium

[1]N.Zimber, [1]P.Vladimirov

[1]Karlsruhe Institute of Technology (KIT), Institute for Applied Materials – Applied Materials Physics (IAM-AWP), Herman-von-Helmholtz-Platz 1, 76344 Eggenstein-Leopoldshafen, Germany

Corresponding author: Nikolai Zimber

Address: Karlsruhe Institute of Technology (KIT), Institute for Applied Materials – Applied Materials Physics (IAM-AWP), Herman-von-Helmholtz-Platz 1, 76344 Eggenstein-Leopoldshafen, Germany

Telephone number: +49 721 608 28540

E-mail address: nikolai.zimber@kit.edu

Keywords: beryllium, denuded zone, tritium retention, neutron irradiation

Graphical Abstract

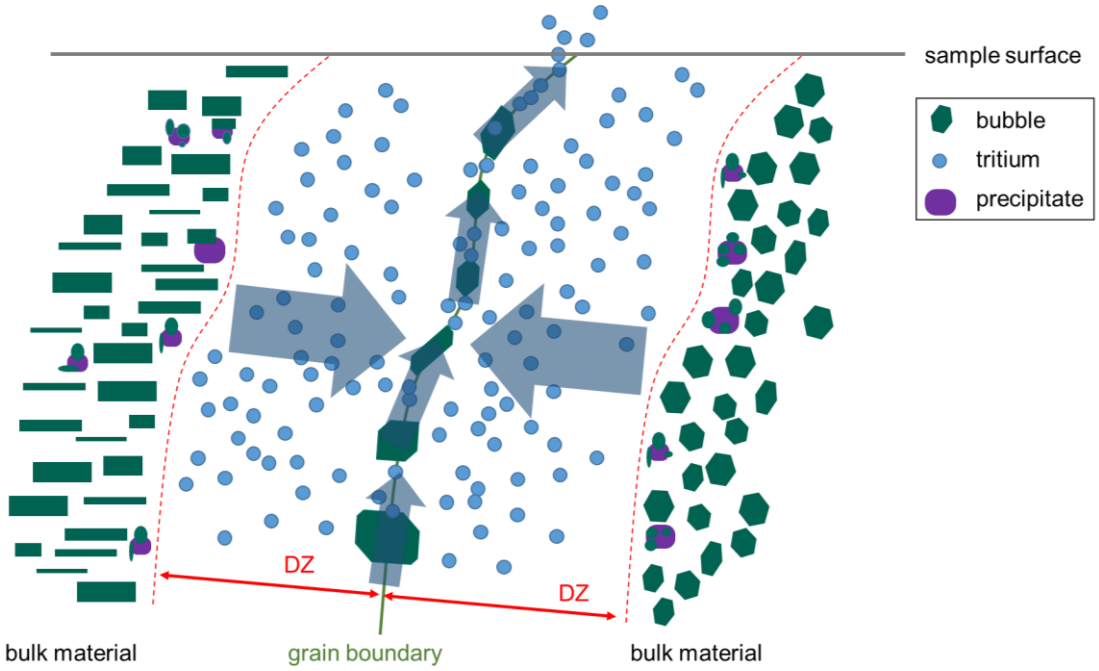

Abstract

1. Introduction

To maintain a sufficiently large tritium breeding rate (TBR) of ≥ 1.1 [1] a neutron multiplier is necessary to keep the neutron flux sufficiently high for the breeding reaction. Besides lead, beryllium is considered suitable for this purpose, since it releases two neutrons with a high probability during the reaction with one neutron. In the helium-cooled pebble-bed (HCPB) design concept developed at the Karlsruhe Institute of Technology (KIT) [2,3] beryllium and a lithium ceramic (Li_4SiO_4) will be placed in alternating layers separated by helium-cooled EUROFER97 plates. Besides the displacement damage, generation of helium and hydrogen will lead to microstructural changes which could result in swelling and a strong tritium retention. For DEMO, it is expected that up to 23.8 kg of tritium can accumulate in 390 t of beryllium [4] This could pose a significant safety risk, as there is a risk that the β-emitter could be partially released in an uncontrolled manner in the event of an accident. However, this must not happen even in the event of a loss of coolant accident (LOCA) or any other disaster scenario. In order to assess the tritium inventory, a fundamental understanding of the evolving microstructure during neutron irradiation is necessary. In the past, a variety of neutron irradiation studies have already been performed. However, these irradiations were performed either at low temperatures (70-400 °C) [5–7] or resulted only in relatively low damage and transmutant gas production (< 2 x 10^{22} cm^{-2}) [8–10]. A selection of all available data for past irradiation campaigns [5,6,8,11–20] is summarized in Figure 1 with respect to temperature and helium production.

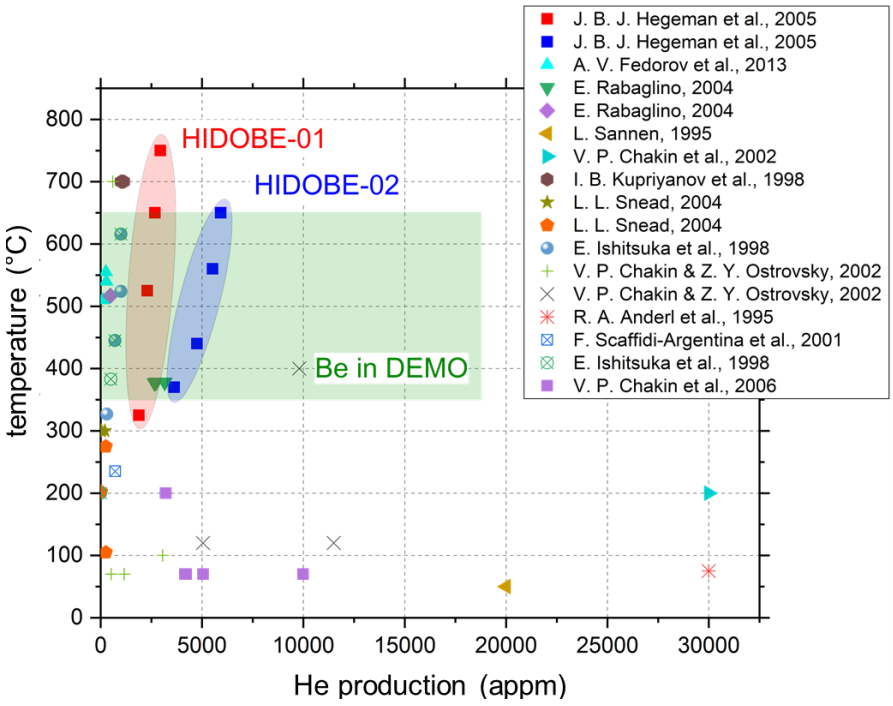

Figure 1: Overview of beryllium irradiation campaigns with reference to the irradiation temperature and helium production. The green area marks the expected damage [4] for beryllium in DEMO. [21]

To simulate fusion conditions that are closer to the ones expected for DEMO the irradiation campaign HIDOBE-02 was performed in the High-Flux Reactor (HFR) in Petten. The four yearlong irradiation campaign has led to a damage of up to 34 dpa and a gas production of 5524 appm He and 596 appm ^{3}H. More details about the irradiation conditions and parameters can be found in [22] and [23]. The microstructural evolution after HIDOBE-01 [24–26] and HIDOBE-02 [23,27] was already extensively studied in earlier publications. From these investigations it is well known that neutron irradiation of beryllium leads to the formation of bubble denuded zones (DZ) around grain boundaries (GB), whereby their width of these zones increases with temperature [23]. Furthermore temperature programmed desorption experiments (TPD) performed with the HIDOBE-02 pebbles revealed a strong tritium trapping [28] even at temperatures (< 450 °C). After irradiation at 600 °C up to 20% of the theoretically produced tritium is still retained within the material (see Figure 2).

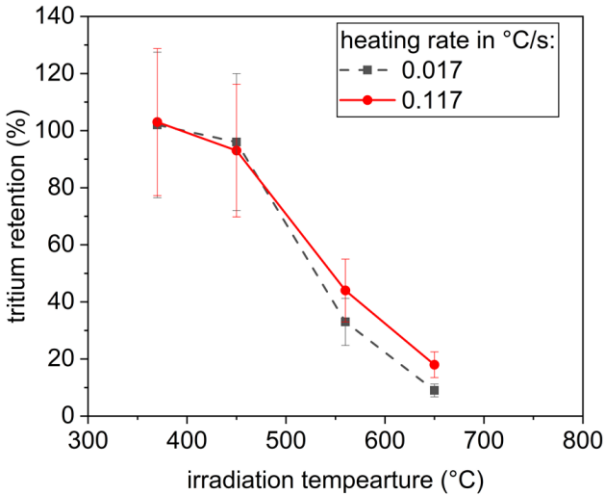

Figure 2: Tritium retention for the 1 mm Be pebbles from HIDOBE-02 in dependence of the heating rate. The released amounts were compared with theoretically calculated values for the ^{3}H accumulation. Data from: [28]. [21]

Until a few years ago it was assumed [11] that tritium which is released from the pebbles during irradiation may originate from any position of the bulk material, i.e. also from bubbles in the grain interior. However, recent EELS analysis [29] proofed the co-existence of helium and tritium within closed bubbles. In addition ab initio calculations [27,30–32] predict a strong tritium trapping within helium bubbles. Barriers for hydrogen desorption into vacuum, i.e. the bubble interior are estimated to be in the range of 0,94-1,52 eV. With up to 3 eV the barrier for diffusion into the bulk material is even higher.[30] It is therefore reasonable to assume that the tritium released during irradiation does not originate from bubbles located in the grain interior as it is irreversible trapped there and may only be released by heating the samples to temperatures > 1100 °C [28] . Instead, the considerations in the present paper suggest that all tritium released during irradiation originates solely from the area of the later DZs. We show this by using a simple self-developed model which first indicates that the formation of the DZs is the result of a reduced point defect concentration in the direct vicinity of the GBs. In the further course of

this publication we then demonstrate that it can be assumed that the whole amount of tritium released during irradiation originates from the later bubble denuded zones. At intermediated temperatures (~487 °C) the release of larger quantities is presumably prevented by the formation of a large number of precipitates that formed directly adjacent to the DZs which are abundant covered with bubbles. The results presented in the proceeding of this paper are part of a thesis [21] that will be published soon something elsewhere.

2. Methods

The investigated Be samples are the same 1 mm *constrained* pebbles that were already used for the studies in [23]. These pebbles were irradiated at 387 °C, 487 °C and 600 °C up to a displacement damage of 34 dpa and gas productions of ~6000 appm He and ~600 appm H during the HIDOBE-02 campaign. In the aforementioned paper details about sample preparation, data acquisition in the TEM and more details about the irradiation conditions can be found. For the microstructural investigations in this paper we focused on the grain boundaries and the areas directly around them.

In order to describe the evolution of the bubble denuded zones during irradiation we developed a simplified model based on classical rate equations. The objective of this model is to determine the change in point defect concentrations around grain boundaries to draw conclusions about the evolution of the denuded zones. For our model we made the following assumptions:

(1) Bubble are the only relevant sinks in the immediate vicinity of grain boundaries or rather have the largest sink strength
(2) The influence of helium on the bubble evolution is neglected as helium only important for bubble nucleation but plays no role in bubble growth
(3) Bubbles have already nucleated and no nucleation takes place anymore.
(4) An average diffusion coefficient is used for the diffusion of SIAs and Vs to account for the anisotropic diffusion.

$$\frac{\mathrm{d}C_\mathrm{v}}{\mathrm{d}t} = K_0 - K_\mathrm{iv}\mathrm{C_i}C_\mathrm{v} - K_\mathrm{is}C_\mathrm{s}C_\mathrm{v},. \quad (1)$$

$$\frac{\mathrm{d}C_\mathrm{i}}{\mathrm{d}t} = K_0 - K_\mathrm{iv}\mathrm{C_i}C_\mathrm{v} - K_\mathrm{vs}C_\mathrm{s}C_\mathrm{i}. \quad (2)$$

Here, C_i and C_v are the vacancy (V) and self-interstitial (SIA) concentrations, K_0 the defect production rate and K_iv the recombination factor which accounts for spontaneous recombination of SIAs and vacancies. Using the atomic volume Ω, average diffusion coefficients D_i and D_v and an interaction radius r_iv the recombination factor can be estimated as follows:

$$K_{\mathrm{iv}} = \frac{4\pi r_{\mathrm{iv}}(D_{\mathrm{i}} + D_{\mathrm{v}})}{\Omega}. \quad (3)$$

The interaction radius r_{iv} can be calculated using equation (4) where $\mathrm{r_a}$ and $\mathrm{r_c}$ represent the size oft the spontaneous recombination zones along the respective lattice direction and are given as zu $\mathrm{r_a}$ = 8.0 x 10^{-10} m and $\mathrm{r_c}$ = 5.0 x 10^{-10} m [33].

$$\mathrm{volume} = \frac{4\pi}{3}\mathrm{r_a}^2\mathrm{r_c} \quad (4)$$

$$r_{\mathrm{iv}} = \sqrt[3]{\mathrm{volume}\frac{3}{4}\frac{1}{\pi}} \quad (5)$$

The loss of point defects to sinks is expressed by a sink strength k_{xs}^2 which can be determined as:

$$k_{\mathrm{is}}^2 = \frac{K_{\mathrm{is}}C_{\mathrm{s}}}{D_{\mathrm{i}}}, \qquad k_{\mathrm{vs}}^2 = \frac{K_{\mathrm{vs}}C_{\mathrm{s}}}{D_{\mathrm{v}}}. \quad (6)$$

For the bubble sink strength we used values from [34]. Their derivation will be puslihed soon elsewhere. The sink densities for each temperature are given by the bubble densities which were already determined in [23]. All parameters used for the calculations in this paper are summarized in Table 1.

Table 1: Overview of the parameters used for the rate equations.

parameter				**unit**
	378 °C	478 °C	600 °C	
V concentration thermal	7,7 x 10^{-7}	4,9 x 10^{-6}	2,4 x 10^{-5}	-
SIA concentration thermal	8,46 x 10^{-33}	1,4 x 10^{-28}	5,7 x 10^{-25}	-
defect production rate	1,91 x 10^{-7}	2,69 x 10^{-7}	3,36 x 10^{-7}	s^{-1}
recombination parameter	9,0 x 10^{13}	1,3 x10^{14}	1,8 x 10^{14}	s^{-1}
sink strength bubble ensemble V [34]	4,6 x 10^{15}	3,8 x 1015	2,15 x 10^{16}	m^{-3}
sink strength bubble ensemble SIA [34]	4,6 x 10^{15}	3,9 x 10^{15}	2,26 x 10^{16}	m^{-3}
Diffusion coefficient V	1,73 x 10^{-12}	9,4 x 10^{-12}	4,0 x 10^{-11}	m^2s^{-1}
Diffusion coefficient SIA	8,3 x 10^{-8}	1,2 x 10^{-7}	1,7 x 10^{-7}	m^2s^{-1}

Grain boundaries are strong sinks for point defects. Due to diffusion kinetics of Vs and SIAs their concentration is lower in the direct vicinity of grain boundaries compared to the grain interior which results in the formation of a concentration gradient. If the local vacancy concentration C_V drops below a critical concentration $c_{\mathrm{krit.}}$, no bubbles form around the grain boundary and a bubble denuded zone os formed [35–37]. On the other hand, an abundance of interstitial atoms along the grain boundary causes it to widen and thus change its position. This affects the size of the DZ. The formation of the DZ as a result of the point defect fluxes to the grain boundary is shown schematically in

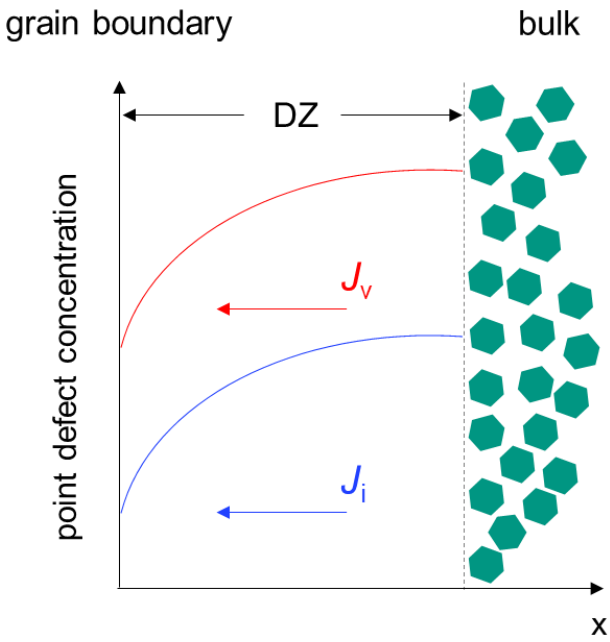

Figure 3: Formation of a bubble denuded zone (DZ) as a result of vacancy (J_v) and interstitial (J_i) fluxes to the grain boundaries.

To estimate the change in grain boundary position as a result of concentration gradients near grain boundaries, the flux of vacancies and interstitial atoms to the interface must first be determined. The flux J of a species is given by

$$J = -D\frac{dC}{dx}. \tag{7}$$

Due to the transport of point defects to the grain boundary, a volume change occurs and the KG position may change. The change in position depends on whether the flux of vacancies J_v or interstitial atoms J_i dominates. The total flux J_{total} of vacancies and interstitial atoms to the grain boundary can then be expressed as

$$J_{\text{total}} = J_{\text{i}} - J_{\text{v}} = -\frac{D_{\text{i}} C_{\text{i}}^{\max}}{dx} + \frac{D_{\text{v}}(C_{\text{v}}^{\max} - C_{\text{v}}^{\text{eq}})}{dx} \tag{8}$$

where the concentration of vacancies and interstitials at the GB is the thermal equilibrium concentration C^{eq}. For SIA $C_{\text{i}}^{\text{eq}} = 0$, for vacancies the equilibrium concentration can by determined in dependence of the temperature T as $C_{\text{v}}^{\text{eq}} = \exp\left(\frac{-E_{\text{v}}^{\text{f}}}{k_{\text{B}} T}\right)$. The vacancy formation energy E_{v}^{f} in beryllium is 0,8 eV [38], and the Boltzmann constant k_B 8,617 x 10^{15} eV/K. $C_{\text{i}}^{\max}$ und $C_{\text{v}}^{\max}$ are the maximum point defect concentrations in the grain interior due to the irradiation. The time dependent evolution of the point defect concentrations is given by:

$$\frac{dC}{dt} = -\nabla J = -\frac{d}{dx}\left(D\frac{dC}{dx}\right) \tag{9}$$

Conservation of volume over time implies

$$\frac{dV}{dt} = \left(\frac{dC_\mathrm{i}}{dt} - \frac{dC_\mathrm{v}}{dt}\right)\Omega = S\frac{dx}{dt}. \tag{10}$$

As a consequence the volume change as a result of the diffenret point defect fluxes is obtained by integrating $\nabla J_{\mathrm{total}}$ over the entire volume:

$$\frac{dV}{dt} = S\frac{dx}{dt} = -S\,\Omega\left(D_\mathrm{v}(C_\mathrm{v}^{\max} - C_\mathrm{v}^{\mathrm{eq}}) - D_\mathrm{i}C_\mathrm{i}^{\max}\right)\frac{1}{dx}. \tag{11}$$

Here S represents the spatial y and z coordinates.. Ω is the volume of a beryllium atom. Finally, rearranging equation (12) gives the change in GB position x_c due to the concentration gradient of the point defects.

$$x_\mathrm{c} = \sqrt{2\Omega\left(D_\mathrm{v}(C_\mathrm{v}^{\max} - C_\mathrm{v}^{\mathrm{eq}}) - D_\mathrm{i}C_\mathrm{i}^{\max}\right)t} \tag{12}$$

t is the total irradiation time during the HIDOBE-02 campaign. Furthermore, according to [39], the size of the DZ as a result of the reduced point defect concentration around the KG, x_D, can be estimated as follows:

$$x_\mathrm{D} = \left(\frac{D_\mathrm{v}}{4K_0\mu_\mathrm{iv}}\right)^{\frac{1}{4}}. \tag{13}$$

It was assumed that the diffusion of interstitial atoms and vacancies to the grain boundaries is equal, so that $D_\mathrm{v}(C_\mathrm{v}\text{-}C_{\mathrm{v}0}) = D_\mathrm{i}(C_\mathrm{i}\text{-}C_{\mathrm{i}0})$ where $C_{\mathrm{v}0}$ and $C_{\mathrm{i}0}$ are the vacancies and SIA are equilibrium concentrations. Furthermore, it is assumed that the bubble concentration, but not the bubble size, significantly affects the point defect concentration. The coefficient μ_{iv} is given as the quotient of K_{iv} and $\mathrm{D_v}$. The total size of the DZ is then given by

$$x_{\mathrm{DZ}} = x_\mathrm{c} + x_\mathrm{D}. \tag{14}$$

To determine the steady-state point defect concentration due to irradiation, equations (1) and (2) were solved numerically using a self-developed Matlab code.

3. Results

3.1 Modelling

The time dependent evolution of the vacancy C_i and interstitial atom concentrations C_v for the three different temperatures is shown in Figure 4.

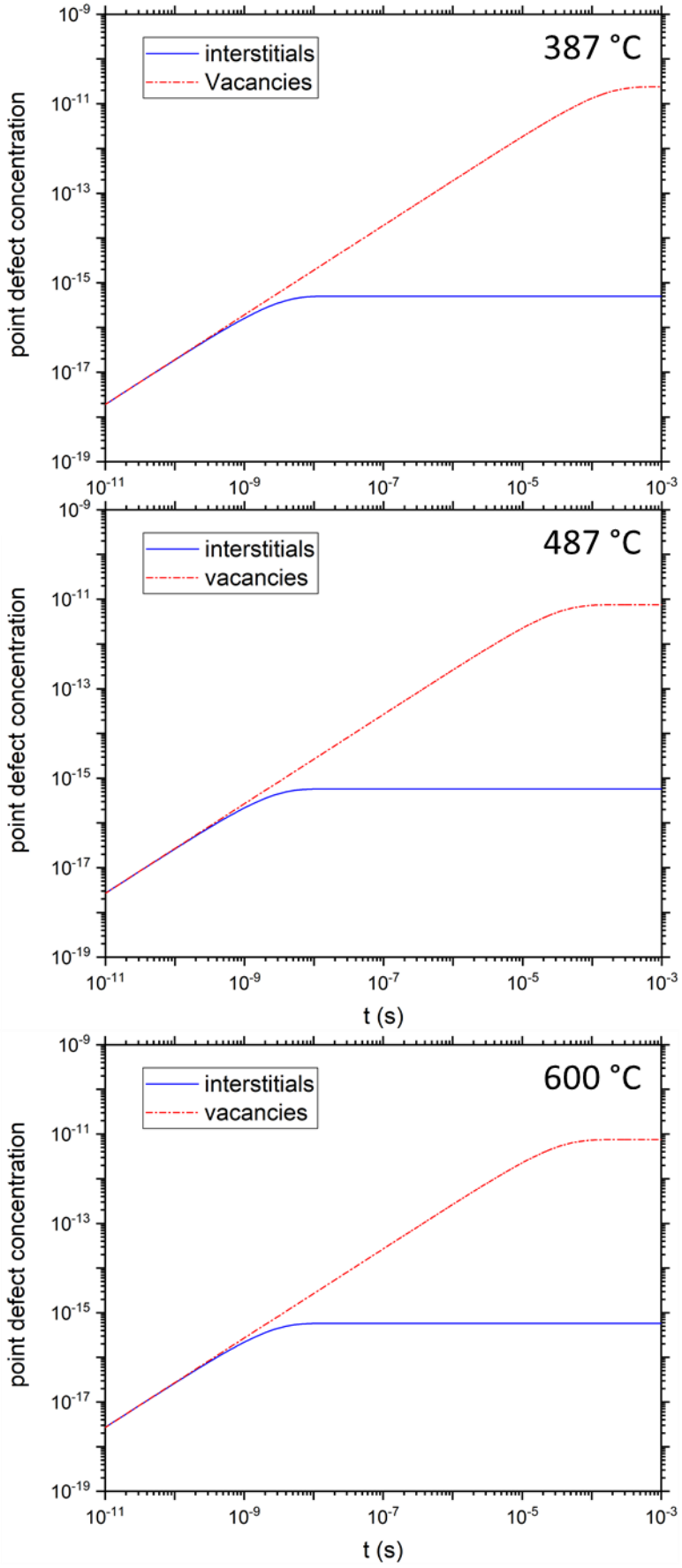

Figure 4: Calculated point defect concentrations, which are characteristic of the irradiation conditions of the constrained 1 mm samples during HIDOBE-02. [21]

It should be noted that the time evolution of the point defect concentrations does not take into account the presence of thermal vacancies. Using the interstitial atom and vacancy concentration values, equations (13) and (14) can be used to determine the increase in DZ as a result of the concentration gradients x_C and due to the decreased point defect concentration x_D. The values are summarized in Table 2 together with the maximum measured values of the DZ, λ_{DZ}. It can be seen that the concentration gradient of the point defects plays only a vanishingly small role and has virtually no influence on the magnification of the DZ. In contrast, the reduced point defect concentration in the immediate KG environment is apparently the main cause for the formation of the DZs. The calculated values for x_D are all in the same order of magnitude as the maximum values determined experimentally in the TEM and deviate from these by only 10-18 %.

Table 2: Parameters for modelling the size of the denuded zone (DZ).

parameter				**unit**
	387 °C	487 °C	600 °C	
C_i max.	5,0 x 10^{-16}	5,7 x 10^{-16}	1,7 x 10^{-16}	-
C_v max.	2,4 x 10^{-11}	7,5 x 10^{-12}	7,1 x 10^{-13}	-
x_C	2,3 x 10^{-14}	2,2 x 10^{-14}	3,9 x 10^{-14}	nm
x_D	461	646	1278	nm
λ_{DZ} max.	380	580	1500	nm

Apparently, the sink effect of the KG ensures that all point defects, which are initially located in the region of the later DZ, diffuse to the grain boundary and either annihilate or are trapped there. This should be true for vacancies and interstitial atoms as well as He and ^{3}H. Furthermore, the results of the EELS measurements in Section 4.2 show that the tritium formed in the grain interior is pinned within the bubbles present there. Accordingly, it can be assumed that most of the tritium formed in the region of the later DZs diffused in atomic form during irradiation, first to the KGs and then along them to the sample surface. There it may leave the sample as a T_2 molecule. To validate this assumption, the amount of theoretically produced tritium within the DZs can be compared to the amount released during irradiation. For this purpose, the tritium atom density N_T produced during irradiation can first be determined using equation (15). The theoretically produced tritium content in appm is shown in Table 2.2 for all irradiation temperatures.

$$N_T = N_{\text{beryllium}} \times tritium\ content \tag{15}$$

The beryllium atomic density $N_{\text{Beryllium}}$ can be calculated using the Avogadro number N_A, 6,022 x 10^{23} mol^{-1}, the mass density $\rho_{\text{beryllium}}$, 1,84 g/cm^3, and the molar mass $M_{\text{Beryllium}}$, such that:

$$N_{\text{Beryllium}} = \frac{\rho_{\text{Beryllium}}}{M_{\text{Beryllium}}} N_{A.} \tag{16}$$

The molar mass is given by the quotient of the atomic mass of beryllium, 9 u, and the amount of substance n. The amount of tritium produced during irradiation within an average sized grain is given by $N_{\mathrm{T}}^{\mathrm{K}}$:

$$N_{\mathrm{T}}^{\mathrm{K}} = N_{\mathrm{T}} \times V_{\mathrm{grain}}, \tag{17}$$

where the grain is assumed to be a spherical object with radius r so that the volume $V_{\mathrm{grain}} = \frac{4}{3}\pi r^3$ (see Figure 5).

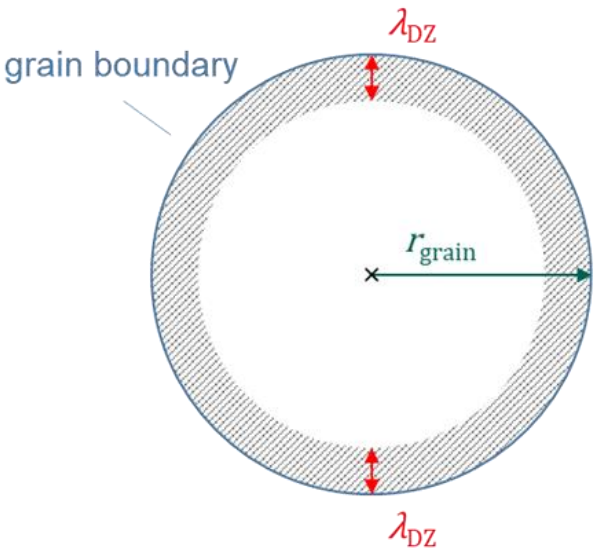

Figure 5: Schematic representation of a grain for calculating the volume of a grain V_{grain} the bubble denuded zone (DZ) V_{DZ} according to equation (19). For the determination of the volume, the DZ was assumed to be a hollow sphere. [21]

Similarly, using the values from TPD measurements [28] the amount of tritium/grain after irradiation $N_{\mathrm{TPD}}^{\mathrm{K}}$ can be determined. The amount of tritium released during irradiation within an average sized grain. $N_{\mathrm{Treleased}}^{\mathrm{K}}$ an be calculated by the difference of the produced amount $N_{\mathrm{T}}^{\mathrm{K}}$ and the amount determined in TPD measurment $N_{\mathrm{TPD}}^{\mathrm{K}}$. The tritium content $N_{\mathrm{T}}^{\mathrm{DZ}}$ within the later DZ can be calculated as follows:

$$N_{\mathrm{T}}^{\mathrm{DZ}} = N_T \times V_{\mathrm{DZ}}. \tag{18}$$

V_{DZ} is given as the volume of a hollow sphere (see Figure 4.30) and defined as follows:

$$V_{DZ} = \frac{4r_{\mathrm{grain}}^3\pi}{3} - \frac{4\left(r_{\mathrm{grain}} - < \lambda_{\mathrm{DZ}} >\right)^3\pi}{3}. \tag{19}$$

The values determined in this way are summarized in Table 3 and graphically presented in. An error of ±20% was assumed for the values, as in [40] ue to the inaccuracies of the TPD measurements and the calculations of the tritium production. On the basis of Figure 6 a good agreement between the amounts of tritium released during irradiation and the theoretically available tritium in the DZ can be seen directly.

Table 3: Parameters used to estimate ^{3}H content within bubble denuded zones. [21]

parameter	symbol				unit
		387 °C	487 °C	600 °C	
^{3}H released during irrad. [28]	-	27	82	416	appm
<grain size>	$<d_{\mathrm{Korn}}>$	6	6	6	µm
<DZ size> (width)	$<\lambda_{\mathrm{DZ}}>$	60	180	1000	nm
^{3}H produced	$N_{\mathrm{T}}^{\mathrm{K}}$	5,12 x 10^9	7,01 x 10^9	10,6 x 10^9	at./grain
^{3}H after irrad.	$N_{\mathrm{TPD}}^{\mathrm{K}}$	4,75 x 10^9	5,86 x 10^9	3,55 x 10^9	at./grain
^{3}H released during irrad.	$N_{\mathrm{Tfrei}}^{\mathrm{K}}$	3,77 x 10^8	1,14 x 10^9	7,10 x 10^9	at./grain
^{3}H in DZ	$N_{\mathrm{T}}^{\mathrm{DZ}}$	3,01 x 10^8	1,19 x 10^9	7,12 x 10^9	at./DZ

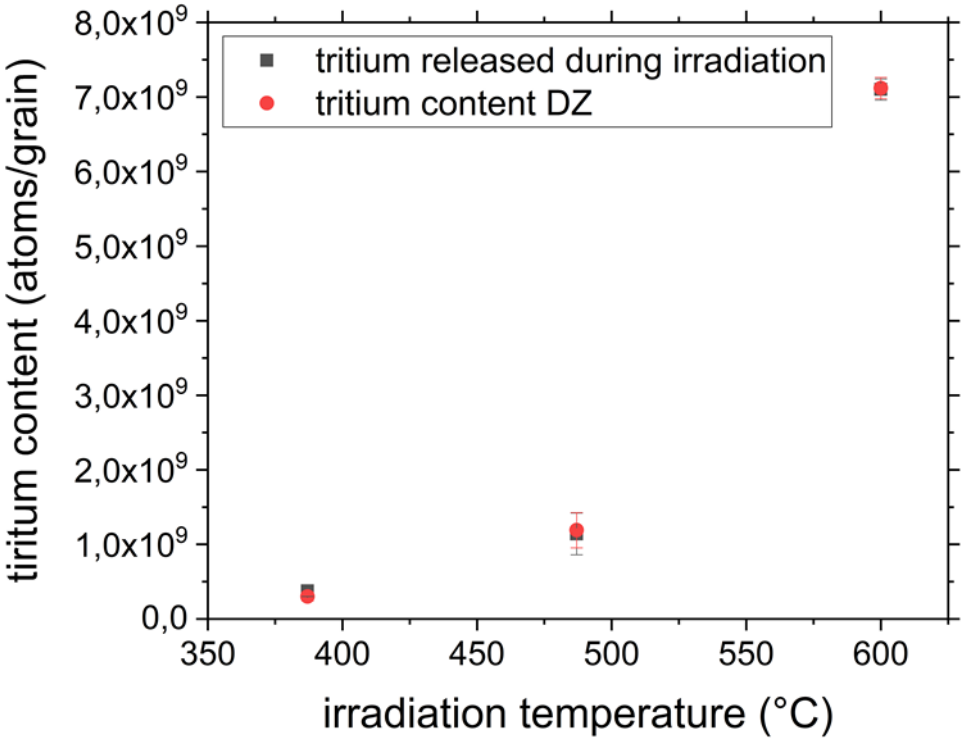

Figure 6: Tritium release during irradiation and theoretical tritium content within the bubble-depleted zone as a function of irradiation temperature. [21]

3.2 Microstructure

As it was already shown in [23] we could observe the formation of bubble denuded zones around grain boundaries at all three irradiation temperatures whereby their size increases with the temperature from an average of 60 nm at 387 °C up to 1000 nm at 600 °C (see Table 3). Figure 7 shows the formation of a bubble denuded zone at 487 °C. Especially at this temperature (see Figure 9) but also at 387 °C (see Figure 8) a large number of precipitate-bubble pairs have formed in the direct vicinity of the DZs. Precipitation densities are summarized for all samples in Table 4. The origin of the bubble accumulation on the precipitation surfaces was already discussed in [23,27] and can be attributed to the strong binding energy ($E_{\mathrm{b}} \approx .0$ eV) of solutes (Al, Si, Mg and He) with vacancies. Solute-vacancy pairs

diffuse through the matrix until they reach a sink where the solute contribute to precipitate formation and the excess vacancies accumulate at the bubble surface.

Table 4: Precipitation densities $\rho_{precipitate}$ and precipitation sizes within irradiated 1 mm constrained beryllium pebbles after the HIDOBE-02 irradiation campaign. [21]

parameter	**temperature**			
	unirr.	387 °C	487 °C	600 °C
$\rho_{precipitations}$ total	2,7 x 10^{19} m^{-3}	1,5 x 10^{19} m^{-3}	7,4 x 10^{19} m^{-3}	8,1 x 10^{17} m^{-3}
$\rho_{precipitations}$ vicinity GB	-	3,6 x 10^{19} m^{-3}	1,5 x 10^{20} m^{-3}	-
max. size precipitate	90 nm	100 nm	450 nm	100 nm
<precipitate>	25 nm	17 nm	22 nm	30 nm

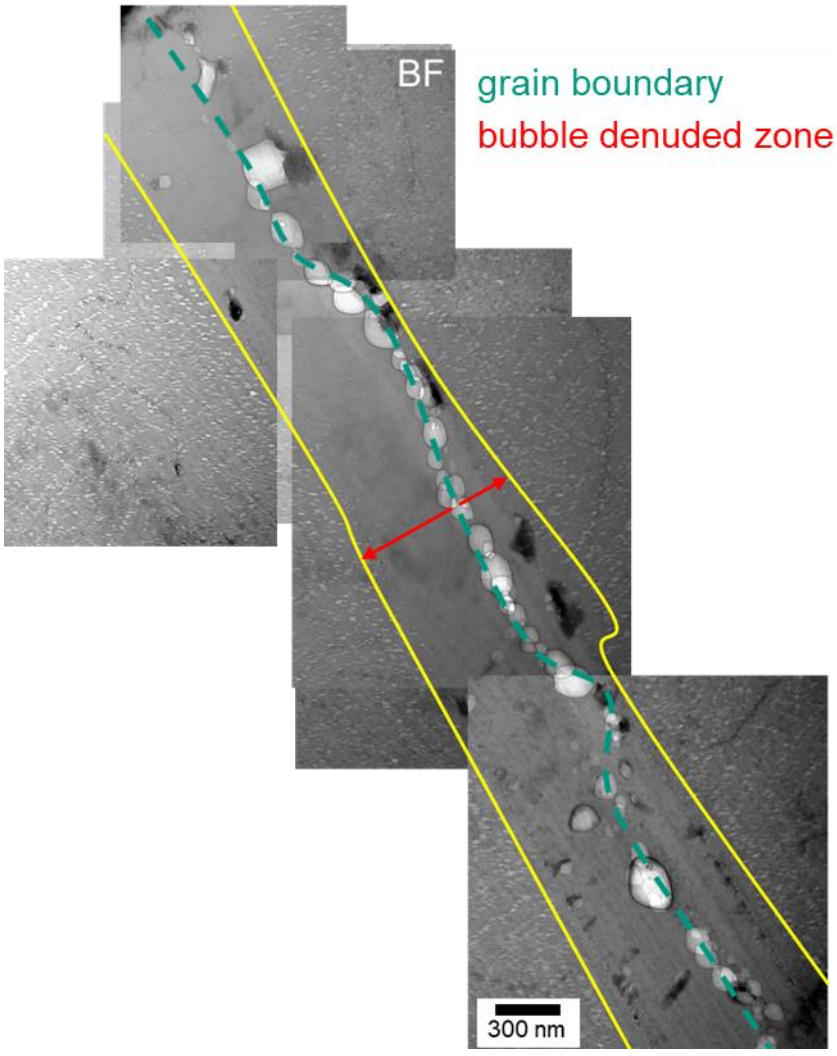

Figure 7: Denuded Zone (DZ) formation around a grain boundary in beryllium irradiated at 487 °C [23].

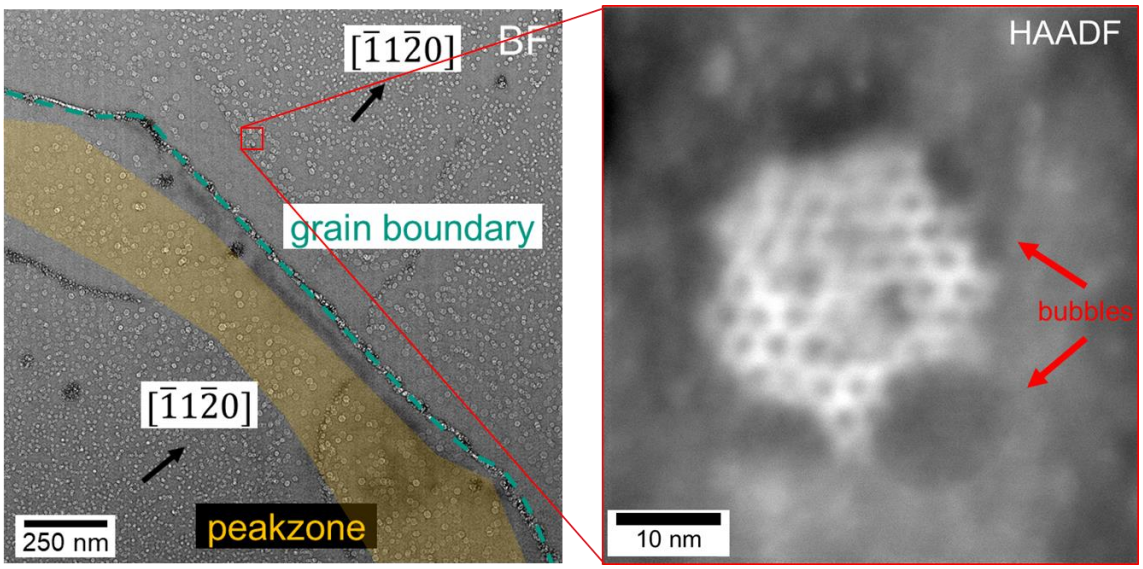

Figure 8: Low angle grain boundary at 487 °C. In the direct vicinity of the denuded zone the number of precipitates covered with bubbles is increased. [21]

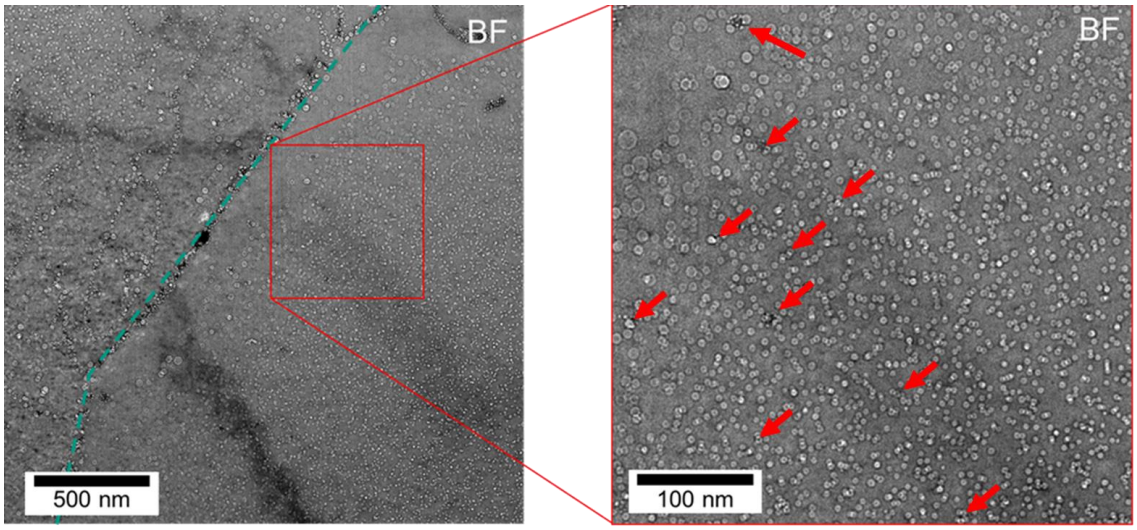

Figure 9: Grain boundary at 387 °C. In the direct vicinity of the denuded zone the number of precipitates covered with bubbles (see red arrows) is increased. [21]

4. Discussion

As the modelling results in chapter 3.1 show, the formation and enlargement of the DZs can be attributed to an effective reduction of the point defect concentration in the immediate vicinity of the grain boundaries. Point defects around the GBs are thus effectively removed by the latter from the grain interior, providing bubble-free areas as nucleation is suppressed. The amount of tritium released during irradiation corresponds approximately to the fraction produced within the later DZs. Once point defects have reached the GB, they may annihilate there or, in all likelihood, leave the sample to a large extent by diffusion along fast paths at grain

boundaries. Thus, it is reasonable to assume that during irradiation, the tritium formed in the later DZs migrates to the grain boundaries as an extremely mobile interstitial atom, unless it is previously trapped at effective sinks. There, it can either leave the sample directly or is initially trapped in bubbles that coalesce into open channels over time during irradiation at temperatures ≥ 600 °C (see Figure 10)

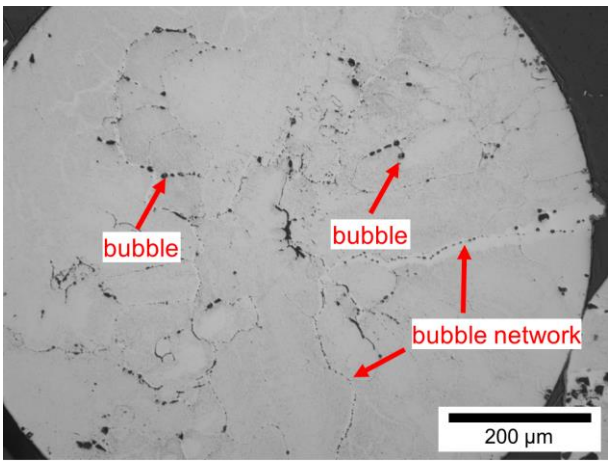

Figure 10: Micrograph under the light microscope of a 1 mm Be constrained pebble after irradiation at 600 °C. Clearly visible bubble and bubble networks that might form open channels have formed during the irradiation. Tritium then escapes through these channels together with helium. However, not all of the tritium produced diffuses to the grain boundaries, as assumed in previous work [68], but only the part formed in their immediate vicinity. The rest remains trapped inside the bubbles in the grain interior and can only be released by heating the samples to > 1100 °C [28].

The amounts of tritium produced in the later DZs correspond at all temperatures approximately to the part which was missing after irradiation compared to the theoretically produced amount (see Figure 6). Accordingly, the tritium retention in beryllium could be significantly improved by a grain structure as fine as possible with grain sizes ≤ 2 λ_{DZ}, i.e. 0,8–3,0 µm, depending on the operating temperature.. Based on the evidence obtained, it can probably be assumed that the release of larger amounts at the two low irradiation temperatures appears to be prevented by precipitation bubble pairs formed inside the grains along the DZs and acting as an additional sink for tritium. Both helium and tritium were detected within gas bubbles along large and small angle grain boundaries (see Figure 4.25 and Figure 4.26), although at lower levels than in the grain interior. As the irradiation progressed, some of the bubbles along the grain boundaries then coalesced into extended networks (see Figure 2.7), which reached the sample surfaces in places, further reducing the tritium content. The total duration for the tritium release can be determined by the so-called *tritium residence time* τ [41], reached the sample surfaces in places, further reducing the tritium content. i.e. the residence time within the sample

$$\tau = \frac{I(T)}{G}, \qquad (20)$$

where $I(T)$ is the tritium inventory after irradiation and G is the tritium production rate. While τ at 387 C is still 1180 days, at 487 °C it is only 1065, at 600 °C even only 424 days. The higher the irradiation temperature, the faster the steady state is reached, where produced and released tritium balance each other. It should be noted that equation (20) applies only to temporary sinks within the DZ, but not to those that permanently trap tritium, as is the case for bubbles in the grain interior.

5. Conclusion

After neutron irradiation of beryllium bubble denuded zones have formed in the immediate vicinity of the grain boundaries, as grain boundaries act as an effective sinks for point defects. The studies in this work suggest that all tritium released during irradiation was produced by neutron induced transmutation in the later DZs and was able to leave the samples by diffusion along the grain boundaries. The release of larger amounts of tritium may have been suppressed at temperatures ≤ 487 °C by intense precipitation-bubble pair formation along the DZs, as the bubbles act as effective tritium sinks. In this way, diffusion of larger amounts of tritium from the grain interior to the grain boundaries is partially prevented.

The results of this work indicate that the tritium retention behavior in beryllium could be significantly improved by two aspects: (i) the use of high purity beryllium could prevent the formation of precipitations during irradiation, which in turn could allow tritium to reach the grain boundaries more easily. However, the production of high-purity beryllium is likely to involve an enormous technical effort, which would be reflected in significantly increased costs. (ii) Since the tritium released during irradiation appears to originate only from the area around the grain boundaries, a grain structure as fine as possible, with grain sizes well below 5-6 µm, should lead to an improvement in tritium release during irradiation. However, the technological implementation is also more cost-intensive here.

Authors Contributions

N.Z. performed the TEM analysis, set up the initial model and wrote the initial draft of this publication. P.V. provided guidance on result analysis and model development.

Acknowledgment

This work has been carried out within the framework of the EUROfusion Consortium and has received funding from the Euratom research and training programme 2014-2018 and 2019-2020 under grant agreement No 633053. The views and opinions expressed herein do not necessarily reflect those of the European Commission.

The research used FIB from the UKAEA's Materials Research Facility, which has been funded by and is part of the UK's National Nuclear User Facility and Henry Royce Institute for Advanced Materials. V.K. contribution work was also partially funded by the RCUK Energy Programme (Grant No. EP/T012250/1).

Data availability

The datasets generated during and/or analysed during the current study are available from the corresponding author on reasonable request.

6. References

[1] M. Rubel, Fusion Neutrons: Tritium Breeding and Impact on Wall Materials and Components of Diagnostic Systems, J Fusion Energ 38 (2019) 315–329. https://doi.org/10.1007/s10894-018-0182-1.

[2] F. Hernández, P. Pereslavtsev, Q. Kang, P. Norajitra, B. Kiss, G. Nádasi, O. Bitz, A new HCPB breeding blanket for the EU DEMO: Evolution, rationale and preliminary performances, Fusion Engineering and Design 124 (2017) 882–886. https://doi.org/10.1016/j.fusengdes.2017.02.008.

[3] F.A. Hernández, P. Pereslavtsev, G. Zhou, B. Kiss, Q. Kang, H. Neuberger, V. Chakin, R. Gaisin, P. Vladimirov, L.V. Boccaccini, G.A. Spagnuolo, S. D'Amico, I. Moscato, Advancements in the Helium-Cooled Pebble Bed Breeding Blanket for the EU DEMO: Holistic Design Approach and Lessons Learned, Fusion Science and Technology 75 (2019) 352–364. https://doi.org/10.1080/15361055.2019.1607695.

[4] Y. Chen, U. Fischer, P. Pereslavtsev, F. Wasastjerna, The EU power plant conceptual study - neutronic design analyses for near term and advanced reactor models: Bericht: FZKA 6763, Karlsruhe, 2003.

[5] L. Sannen, C. de Raedt, F. Moons, Y. Yao, Helium content and induced swelling of neutron irradiated beryllium, Fusion Engineering and Design 29 (1995) 470–474. https://doi.org/10.1016/0920-3796(95)80055-3.

[6] V.P. Chakin, Z.Y. Ostrovsky, Evolution of beryllium microstructure under high-dose neutron irradiation, Journal of Nuclear Materials 307-311 (2002) 657–663. https://doi.org/10.1016/S0022-3115(02)01184-4.

[7] V. Kuksenko, K. Ammigan, B. Hartsell, C. Densham, P. Hurh, S. Roberts, Irradiation effects in beryllium exposed to high energy protons of the NuMI neutrino source, Journal of Nuclear Materials 490 (2017) 260–271. https://doi.org/10.1016/j.jnucmat.2017.04.011.

[8] I.B. Kupriyanov, V.A. Gorokhov, R.R. Melder, Z.E. Ostrovsky, A.A. Gervash, Investigation of ITER candidate beryllium grades irradiated at high temperature, Journal of Nuclear Materials 258-263 (1998) 808–813. https://doi.org/10.1016/S0022-3115(98)00383-3.

[9] E Rabaglino, C Ferrero, J Reimann, C Ronchi, T Schulenberg, Study of the microstructure of neutron irradiated beryllium for the validation of the ANFIBE code, Fusion Engineering and Design 61-62 (2002) 769–773. https://doi.org/10.1016/S0920-3796(02)00149-7.

[10] D.S. Gelles, H.L. Heinisch, Neutron damage in beryllium, Journal of Nuclear Materials 191-194 (1992) 194–198. https://doi.org/10.1016/S0022-3115(09)80032-9.

[11] E. Rabaglino, Helium and Tritium in Neutron-irradiated Beryllium: Bericht FZKA 6939, 2004.

[12] V.P. Chakin, A.O. Posevin, R.N. Latypov, Radiation damage in beryllium at 70–440°C and neutron fluence (0.3–18)·1022 cm−2 (E n > 0.1 MeV), At Energy 101 (2006) 743–749. https://doi.org/10.1007/s10512-006-0162-9.

[13] A.V. Fedorov, S. van Til, L.J. Magielsen, M.P. Stijkel, Analysis of tritium retention in beryllium pebbles in EXOTIC, PBA and HIDOBE-01 experiments, Journal of Nuclear Materials 442 (2013) S472 - S477. https://doi.org/10.1016/j.jnucmat.2013.03.010.

[14] L.L. Snead, Low-temperature low-dose neutron irradiation effects on beryllium, Journal of Nuclear Materials 326 (2004) 114–124. https://doi.org/10.1016/j.jnucmat.2003.12.016.

[15] E. Ishitsuka, H. Kawamura, T. Terai, S. Tanaka, Microstructure and mechanical properties of neutron irradiated beryllium, Journal of Nuclear Materials 258-263 (1998) 566–570. https://doi.org/10.1016/S0022-3115(98)00106-8.

[16] I.B. Kupriyanov, V.A. Gorokhov, V.V. Vlasov, A.M. Kovalev, V.P. Chakin, The effect of helium generation and irradiation temperature on tritium release from neutron irradiated beryllium, Journal of Nuclear Materials 329-333 (2004) 809–813. https://doi.org/10.1016/j.jnucmat.2004.04.282.

[17] S. van Til, J.B.J. Hegeman, H.L. Cobussen, M.P. Stijkel, Evolution of beryllium pebbles (HIDOBE) in long term, high flux irradiation in the high flux reactor, Fusion Engineering and Design 86 (2011) 2258–2261. https://doi.org/10.1016/j.fusengdes.2011.01.079.

[18] F. Scaffidi-Argentina, C. Sand, C. H. Wu, Tritium and Helium Retention in Neutron-Irradiated Beryllium, Physica Scripta T94 (2001) 83. https://doi.org/10.1238/physica.topical.094a00083.

[19] R.A. Anderl, J.D. Baker, G.L. Bourne, R.J. Pawelko, Tritium and Helium Release from Irradiated Beryllium, Fusion Technology 28 (1995) 1114–1119. https://doi.org/10.13182/FST95-A30556.

[20] V.P. Chakin, V.A. Kazakov, R.R. Melder, Y.D. Goncharenko, I.B. Kupriyanov, Effects of neutron irradiation at 70–200 °C in beryllium, Journal of Nuclear Materials 307-311 (2002) 647–652. https://doi.org/10.1016/S0022-3115(02)01218-7.

[21] N. Zimber, Nanoskalige Analytik der Mikrostruktur von hochdosig bestrahltem Beryllium: PhD Thesis, to be published, 2021.

[22] J.B.J. Hegeman, J.G. van der Laan, H. Kawamura, A. Möslang, I. Kupriyanov, M. Uchida, K. Hayashi, The HFR Petten high dose irradiation programme of beryllium for blanket application, Fusion Engineering and Design 75-79 (2005) 769–773. https://doi.org/10.1016/j.fusengdes.2005.06.306.

[23] N. Zimber, P. Vladimirov, M. Klimenkov, V. Kuksenko, Kuksenko, Investigation of a high-dose irradiated beryllium microstructure, Journal of Nuclear Materials 2020.

[24] M. Klimenkov, V. Chakin, A. Moeslang, R. Rolli, TEM study of impurity segregations in beryllium pebbles, Journal of Nuclear Materials 455 (2014) 660–664. https://doi.org/10.1016/j.jnucmat.2014.08.030.

[25] M. Klimenkov, V. Chakin, A. Moeslang, R. Rolli, TEM study of beryllium pebbles after neutron irradiation up to 3000appm helium production, Journal of Nuclear Materials 443 (2013) 409–416. https://doi.org/10.1016/j.jnucmat.2013.07.050.

[26] M. Klimenkov, J. Hoffmann, P. Kurinsky, V. Kuksenko, P. Vladimirov, V. Chakin, A. Möslang, TEM characterization of irradiated beryllium, Konferenzabstract für European Microscopy Congress 2016, Lyon, in: European Microscopy Congress 2016: Proceedings, 2016, pp. 880–881.

[27] M. Klimenkov, P. Vladimirov, U. Jäntsch, V. Kuksenko, R. Rolli, A. Möslang, N. Zimber, New insights into microstructure of irradiated beryllium based on experiments and computer simulations, Scientific reports 10 (2020) 8042. https://doi.org/10.1038/s41598-020-64654-5.

[28] V. Chakin, R. Rolli, M. Klimenkov, M. Zmitko, Tritium release and retention in beryllium pebbles irradiated up to 640 appm tritium and 6000 appm helium, Journal of Nuclear Materials 542 (2020) 152521. https://doi.org/10.1016/j.jnucmat.2020.152521.

[29] M. Klimenkov, P. Vladimirov, J. Hoffmann, N. Zimber, A. Möslang, V. Kuksenko, First simultaneous detection of helium and tritium inside bubbles in beryllium, Micron (Oxford, England 1993) 127 (2019) 102754. https://doi.org/10.1016/j.micron.2019.102754.

[30] C. Stihl, P.V. Vladimirov, A. Möslang, Assessment of multiscale hydrogen desorption models from (0001) Be surfaces, Journal of Nuclear Materials 543 (2021) 152595. https://doi.org/10.1016/j.jnucmat.2020.152595.

[31] M.G. Ganchenkova, P.V. Vladimirov, V.A. Borodin, Vacancies, interstitials and gas atoms in beryllium, Journal of Nuclear Materials 386-388 (2009) 79–81. https://doi.org/10.1016/j.jnucmat.2008.12.063.

[32] M.G. Ganchenkova, V.A. Borodin, R.M. Nieminen, Hydrogen in beryllium: Solubility, transport, and trapping, Phys. Rev. B 79 (2009) 1047. https://doi.org/10.1103/PhysRevB.79.134101.

[33] C. Stihl, Skalenübergreifende Simulation von Wasserstoffisotopen auf (0001) Berylliumoberflächen: Dissertation, DOI: 10.5445/IR/1000090436, Karlsruhe, 2019.

[34] S. Kovalsky, Unpublished calculations of the sink strenght of bubble ensembles, 2020.

[35] B.N. Singh, A.J.E. Foreman, On Transport of Helium to Grain Boundaries during Irradiation: Risø-M; No. 2612, 1986.

[36] B.N. Singh, Foreman A. J. E., Calculated grain size-dependent vacancy supersaturation and its effect on void formation, The Philosophical Magazine: A Journal of Theoretical Experimental and Applied Physics 29 (1974) 847–858. https://doi.org/10.1080/14786437408222075.

[37] I.J. Beyerlein, M.J. Demkowicz, A. Misra, B.P. Uberuaga, Defect-interface interactions, Progress in Materials Science 74 (2015) 125–210. https://doi.org/10.1016/j.pmatsci.2015.02.001.

[38] M.G. Ganchenkova, V.A. Borodin, Ab initio study of small vacancy complexes in beryllium, Phys. Rev. B 75 (2007) 603. https://doi.org/10.1103/PhysRevB.75.054108.

[39] Konobeev Yu. V., Subbotin A. V., Bykov V. N., Tscherbak V. I., Grain boundary void denuded zone in irradiated metals, physica status solidi (a) 29 (1975) K121-K124. https://doi.org/10.1002/pssa.2210290246.

[40] V. Chakin, R. Rolli, R. Gaisin, U. Hoeppener-Kramar, M. Nakamichi, M. Zmitko, Tritium release and retention in beryllium and titanium beryllide after neutron irradiation up to damage doses of 23-38 dpa, Fusion Engineering and Design 161 (2020) 111938. https://doi.org/10.1016/j.fusengdes.2020.111938.

[41] H. Kwast, R. Conrad, S.D. Preston, G. Verstappen, N. Roux, S. Casadio, H. Werle, J.D. Elen, Comparison of the tritium residence time of various ceramic breeder materials irradiated in exotic experiments 4 and 5, in: Fusion Technology 1990, Elsevier, 1991, pp. 847–851.